Structural, electrical and magnetic characterization of artificial ferromagnetic/superconducting ($La_{0.7}Ca_{0.3}MnO_3/YBa_2Cu_3O_{7-x}$) heterostructures

2009 J. Phys.: Condens. Matter 21 254205

(http://iopscience.iop.org/0953-8984/21/25/254205)

IOP PUBLISHING JOURNAL OF PHYSICS: CONDENSED MATTER

J. Phys.: Condens. Matter **21** (2009) 254205 (7pp) doi:10.1088/0953-8984/21/25/254205

Structural, electrical and magnetic characterization of artificial ferromagnetic/superconducting ($La_{0.7}Ca_{0.3}MnO_3/YBa_2Cu_3O_{7-x}$) heterostructures

S Piano[1,2,3], A De Santis[1,2], F Bobba[1,2], F Giubileo[1,2], M Longobardi[1,2], A Di Bartolomeo[1], M Polichetti[1,2], A Scarfato[1,2], D Zola[1,2], A Vecchione[1,2] and A M Cucolo[1,2]

[1] Physics Department 'E R Caianiello', University of Salerno, Via S. Allende, 84081 Baronissi (SA), Italy

[2] Laboratorio Regionale SUPERMAT, CNR-INFM, Via S. Allende, 84081 Baronissi (SA), Italy

[3] School of Physics and Astronomy, University of Nottingham, Nottingham NG7 2RD, UK

E-mail: samanta@sa.infn.it

Received 20 March 2009
Published 29 May 2009
Online at stacks.iop.org/JPhysCM/21/254205

Abstract

The fabrication and characterization of superconducting and ferromagnetic heterostructures is an open field due to the fundamental interest in the physics of the coexistence of these two competing orders and their possible applications in the spintronics industry. In this paper we present structural, electrical and magnetic characterization for the single $La_{0.7}Ca_{0.3}MnO_3$ (LCMO) thin layer, $La_{0.7}Ca_{0.3}MnO_3/YBa_2Cu_3O_{7-x}$ (LCMO/YBCO) bilayers and the LCMO/YBCO/LCMO trilayers. In particular, we show a detailed magnetic characterization of the LCMO thin films by means of low temperature magnetic force microscopy. We discuss the different dynamics of the magnetic domains observed, depending on the substrate induced strain and on the film thickness.

(Some figures in this article are in colour only in the electronic version)

1. Introduction

According to the BCS theory of superconductivity, the conduction electrons in a metal cannot be both ferromagnetically ordered and superconducting. In fact the superconductors expel the magnetic field passing through them and strong magnetic fields kill the superconductivity (Meissner effect [1]). Even small amounts of magnetic impurities are usually enough to eliminate the superconducting phase. Therefore the striking demonstration of a possible coexistence between magnetic and superconducting orders opens an entire new field of research. The investigation of hybrid superconducting/ferromagnetic heterostructures is aimed at understanding the mechanism of electronic transport in the presence of competing superconducting and ferromagnetic orders. This research also has potential technological outlets in the context of spintronics [2]. A major step forward in the field has been obtained with the discovery of perovskite manganites which exhibit colossal magnetoresistance (CMR) [3]. It has been verified that colossal magnetoresistance manganites have good structural compatibility with high-T_C superconductors, so the research turns naturally towards these systems. Alongside the technological aspect of these systems, interest exists in understanding the features of the superconducting order parameter and its modifications due to the simultaneous presence of a competing magnetic order.

In this work we report the study of the interplay between superconductivity and ferromagnetism in artificial

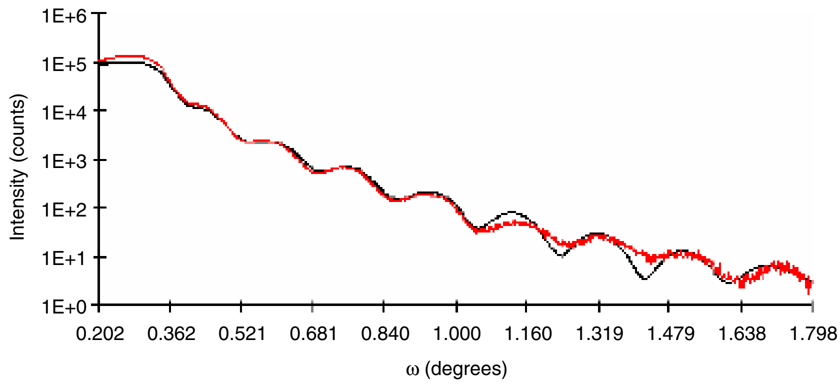

Figure 1. Experimental data (red line) and simulation (black line) for a sample where the expected LCMO thickness was 226 Å.

heterostructures constituted by a high-T_C superconductor, $YBa_2Cu_3O_{7-x}$ (YBCO) and a colossal magnetoresistance material, $La_{0.7}Ca_{0.3}MnO_3$ (LCMO). Before explaining the experimental works carried out on ferromagnetic/superconducting (S/F) systems, we explain the details of the fabrication and characterization of the LCMO. In particular the structural, electrical and magnetic properties of our LCMO samples are presented. Then, we describe the S/F hybrid systems. Also in this case we show the structural, electrical and magnetic measurements.

2. Fabrication and characterization of $La_{0.7}Ca_{0.3}MnO_3$ thin films

The LCMO thin films were grown on (001) $SrTiO_3$ single crystal substrates 5 × 5 mm^2 by a multi-target DC sputtering in high oxygen pressure. During the deposition the substrate temperature was kept at 900 °C and the oxygen pressure at 3.0 mbar. After the deposition the sample was cooled down at 20 °C min^{-1} to room temperature. We performed preliminary tests by varying the pressure and the temperature of the substrates, and eventually the optimal values were selected in order to guarantee the highest metal–insulator transition temperature and a good epitaxiality of the sample [4–6].

We performed x-ray reflectivity of LCMO/STO thin films and the deposition rate was extracted by fitting the experimental data (figure 1); in our case the deposition rate was estimated in 2.7 Å min^{-1}.

Figure 2 shows resistance versus temperature measurements for different thicknesses (16, 40 and 65 nm) of the LCMO layer. These measurements are evidence of a variation of the metal–insulator temperature (T_{MI}) from 166 to 190 K and a reduction of the resistivity with the thickness of the LCMO layer.

The cause of the reduction of T_{MI} with the thickness of the LCMO is an open question. Ziese *et al* [7], investigating the magnetic and magnetotransport properties of LCMO thin films as a function of the thickness, found that the reduction of the film thickness leads to a systematic decrease of the T_{MI} values. They attributed this to the different strain state: fully relaxed above 100 nm and coherently strained under 70 nm on an STO substrate. Rao *et al* [8] have tried to explain the results

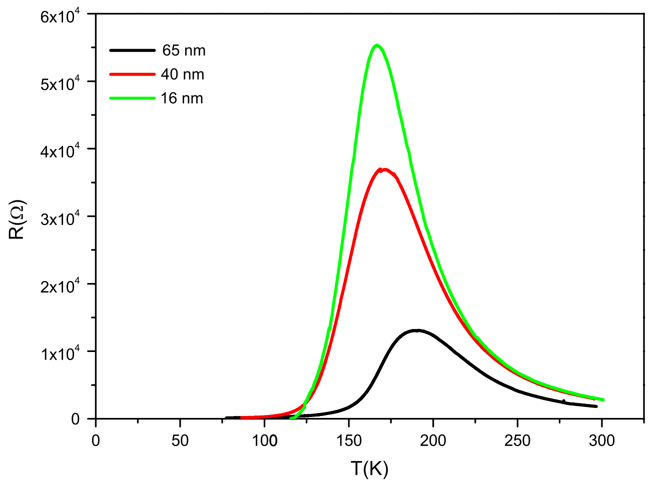

Figure 2. R versus T for different LCMO thicknesses; we can see a variation of the T_{MI}.

obtained for LCMO films with this model but they found no correlation between the strain and the reduction of the value of T_{MI}. They suggested that the transition temperatures can also be influenced by other factors, such as inhomogeneities and disorder in the film. In any case the strain cannot be the only factor responsible for the reduction of T_{MI} in very thin films, in fact the decrease of T_{MI} with the reduction of thickness, happens either for films with a gradually relaxed structure or for fully strained films [9].

We note that an increase of the metal–insulator transition temperature is obtained in the annealed film, in particular, the value of T_{MI} increases up to 260 K which is just the bulk temperature, but a detailed discussion is beyond the scope of this paper, for additional details see [10].

We have also studied the crystalline structures of an LCMO sample, 30 nm thick, through x-ray measurements. From $\theta/2\theta$ analysis, see figure 3, we observe that only (00l) STO and (00l) LCMO reflections appear, indicating that the LCMO films grow preferentially oriented with the c-axis normal to the substrate and there are no spurious phases. To have an estimation of the epitaxiality of the samples we have carried out measurements of the rocking curves. The rocking curve measurements have been performed on the (002)

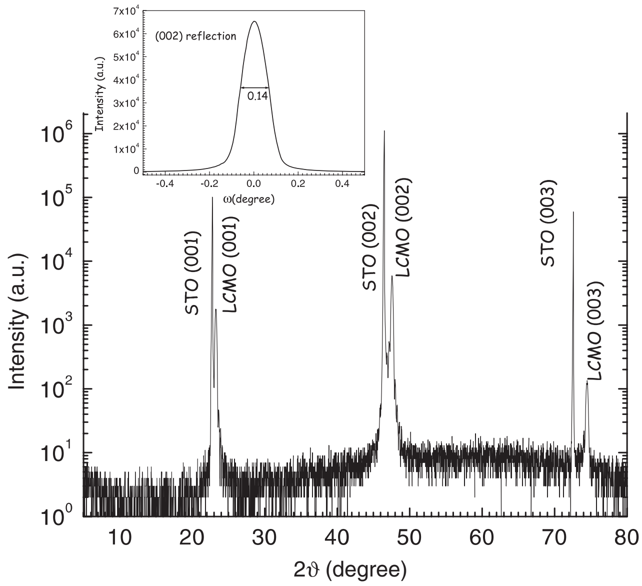

Figure 3. $\theta/2\theta$ measurements of an as grown and annealed sample. Inset: rocking curve of the (002) reflection of LCMO thin film.

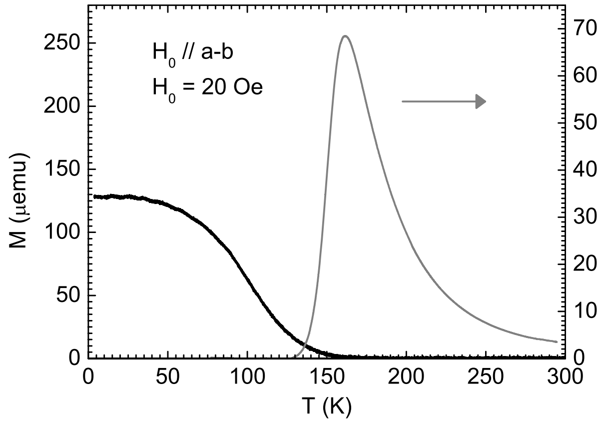

Figure 4. M versus T behavior for a LCMO thin film in a magnetic field of 20 Oe (black line), R versus T of the same film (gray line).

diffraction peak. As shown in the inset of figure 3, we found that the full width at half maximum (FWHM) of the film is 0.14°.

We have also studied the modification of the resistance by applying an external magnetic field. The magnetization as function of the temperature has been measured by placing the thin films in an external magnetic field (H) parallel to the sample surface in such way as to neglect the demagnetizing effects. As shown in figure 4, the magnetization in 20 Oe does not show a sharp ferromagnetic transition. From the magnetization we infer a Curie temperature (T_C) in good agreement with the $T_{MI} \simeq 170$ K, measured by transport properties.

2.1. Magnetic force microscopy

Here we report the characterization by magnetic force microscopy (MFM) at low temperature of the magnetic microstructure of ferromagnetic LCMO thin films. It is well known that the lattice strain due to film-substrate mismatch, inducing magnetostriction, strongly affects the magnetotransport properties of LCMO thin films influencing their physical properties such as the metal-insulating transition, the Curie temperature and the magnetoresistance. Indeed, due to the very low orbital momentum of the bulk LCMO system, the intrinsic magnetocrystalline anisotropy energy of the system is almost negligible and the strain induced magnetostriction, together with the magnetostatic shape anisotropy, dominates the anisotropy energies. This reveals an easy magnetization axis along the directions where the tensile strain takes place. At same time by increasing the film thickness, the shape anisotropy, i.e. the unbalance between volume and surface, is reduced and the in-plane magnetization tendency is lowered. LCMO thin films on $LaAlO_3$ (LAO), $NdGaO_3$ (NGO) and $SrTiO_3$ (STO) substrates were deposited, as described above, in the same sputtering deposition run to avoid growth condition discrepancies. Due to the lattice mismatch between LCMO and the substrates, the bulk lattice constant a of 3.867 Å becomes 3.905, 3.791 and 3.854 Å in LCMO films on STO, LAO and NGO substrates, respectively. This means that LCMO thin films grown on LAO substrates experience a uniaxial tensile strain, which produces a perpendicular out-of-plane easy axis. The samples grown on STO and NGO experience in-plane biaxial tensile strain and in-plane uniaxial tensile strain, which leads to a biaxial easy in-plane anisotropy for STO and an uniaxial easy axis in-plane for NGO. The samples grown on STO and NGO experience, respectively, biaxial and uniaxial in-plane tensile strain, which leads to in-plane easy axes, but, while for NGO the easy axis has a well defined direction, for STO two in-plane easy axes should occur simultaneously.

We performed MFM experiments, following the sample stray field, at various temperatures above films grown on different substrate materials and for different film thicknesses. A perpendicular with respect to the film plane, external magnetic field was used to image the magnetic hysteresis. All the MFM measurements were carried out in frequency modulation detection mode, i.e. the MFM signal was proportional to the out-of-plane component of the force gradient that arose from a long range magnetostatic coupling between the tip and the sample. Commercial Veeco low moment probe tips coated with a magnetic thin film of Co/Cr were used. Finally during scanning, the magnetic tip was lifted to an height of 50–100 nm, flying above the sample surface to follow the sample average slope. Measurements were acquired at low temperature 10–60 K well below the measured metal-insulating transition T_{MI}. In figure 5 the MFM comparison between 100 nm nominal thick LCMO/STO, LCMO/ALO and LCMO/NGO thin films is shown.

In the LCMO/LAO films a clear mazelike pattern of up and down oriented domains is observed, consistent with a perpendicular anisotropy. Further, the in-plane uniaxial strain for LCMO/NGO creates a large out-of-plane magnetization with a typical stripe domain pattern. On STO, we observe that the magnetic structures are larger, more irregular and do not occur in dark–bright pairs.

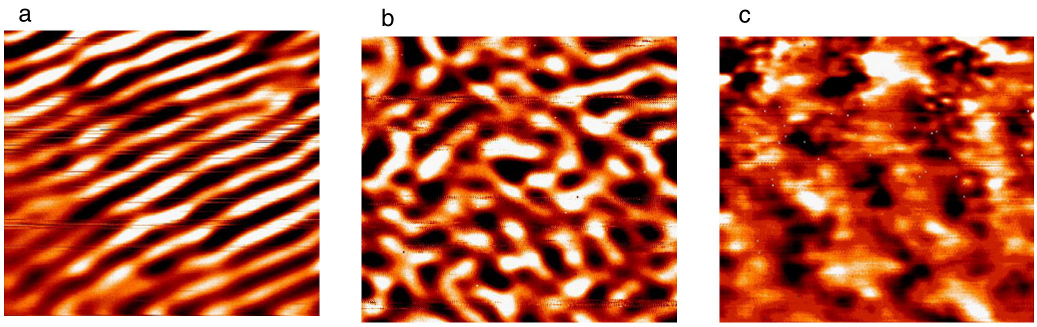

Figure 5. MFM on LCMO thin films on NGO (a), LAO (b) and STO (c).

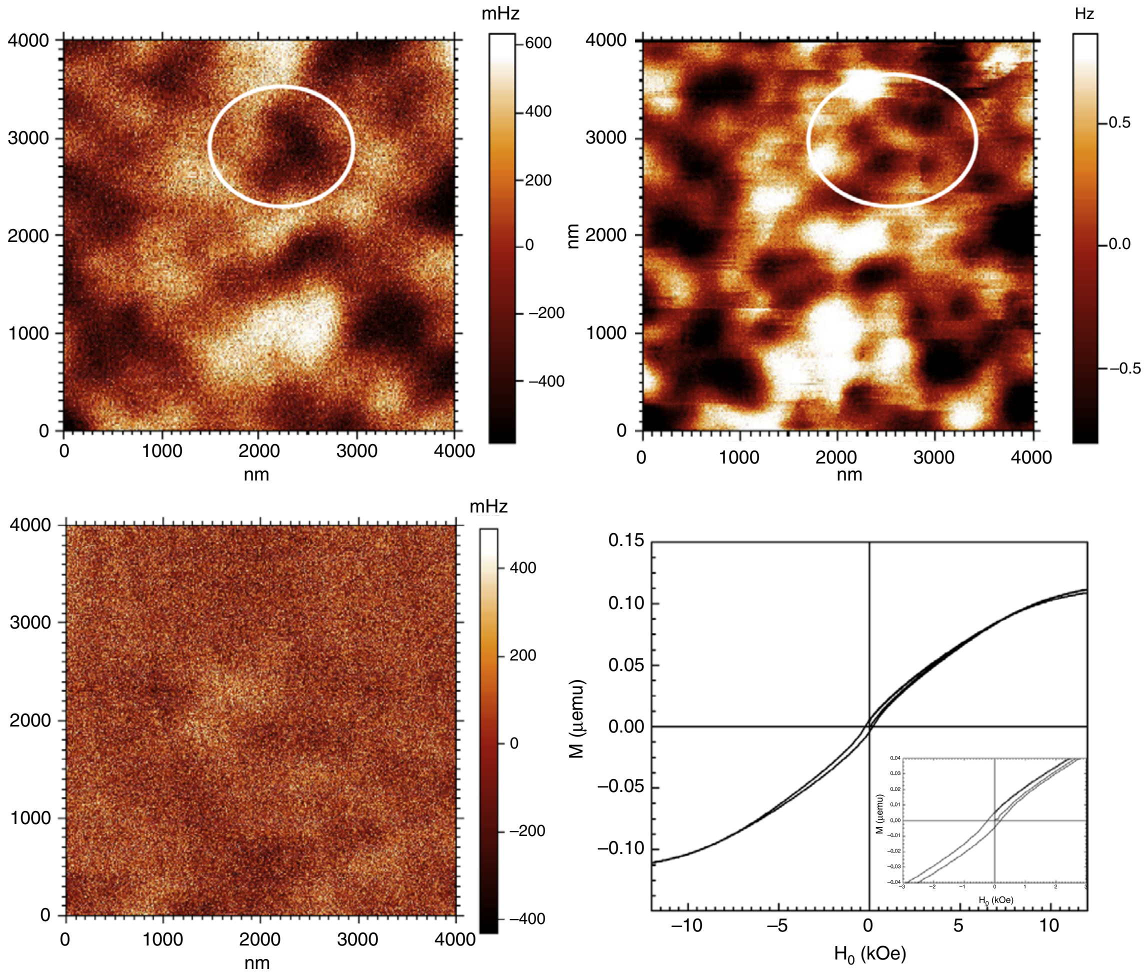

Figure 6. MFM image in a magnetic field $H = 0$ T (a), $H = 0.2$ T (b) and $H = 2$ T (c). The hysteresis loop (c).

In LCMO/STO the magnetostatic stabilization of domains in a checker-board configuration is expected, but irregularities due to the generation of a variety of defects at larger thicknesses, when the lattice strain relaxes, leads to domain deformation. We measured this peculiar checker-board configuration when an external perpendicular field, of sufficient strength, was applied and we observed that thick LCMO/STO domains may collapse into magnetic stripes or bubbles as well as into an isolated ring domain (not reported here for brevity).

Because in this paper we report the characterization of LCMO/YBCO bilayers and trilayers deposited on STO substrates with the LCMO thickness ranging between 10 and 30 nm, we focus, in this context,our attention on the MFM measurements performed on 20 nm of LCMO deposited on STO. In figure 6, the MFM versus H investigation is summarized. Image areas of $5 \times 5\ \mu\text{m}^2$ were acquired at $T = 10$ K working in lift mode with a tip–surface elevation of 50 nm. A magnetic field $H = 2$ T, perpendicular to the film plane, was applied before starting the measurements.

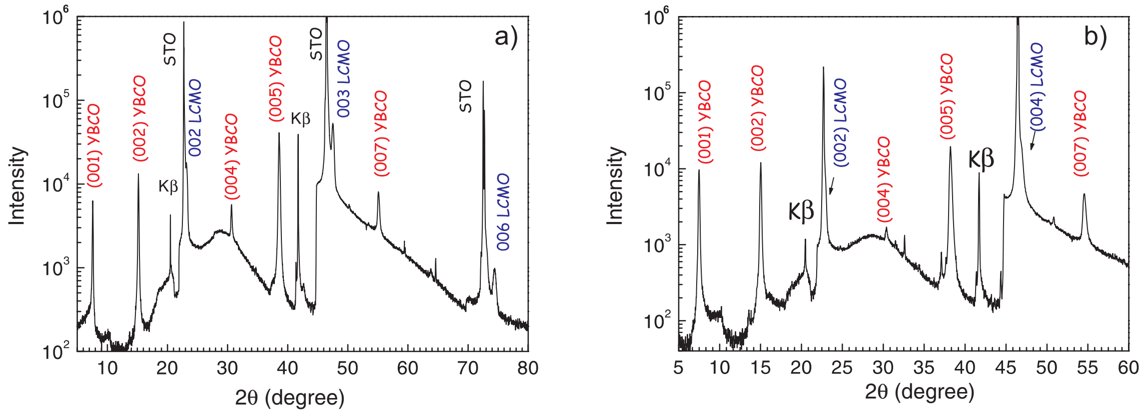

Figure 7. $\theta/2\theta$ measurements on LCMO/YBCO (a) and YBCO/LCMO (b) bilayers.

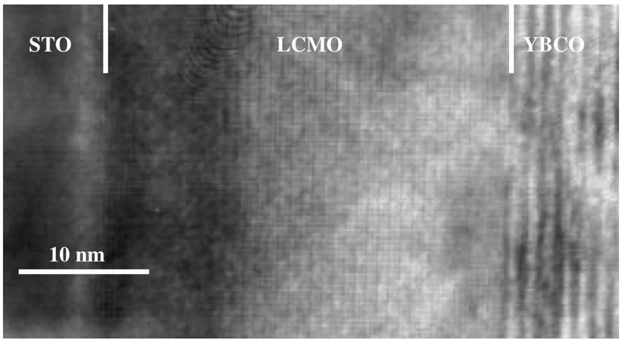

Figure 8. $\theta/2\theta$ measurements on LCMO/YBCO (a) and YBCO/LCMO (b) bilayers.

In figure 6(a) the sample is at the residual magnetization ($H = 0$). We can observe an irregular magnetic low contrast indicating that, on the image scanned area, the magnetization wants to come back to the preferred in-plane configuration. In some regions canted and/or out-of-plane domains appear, exhibiting a magnetic contrast by painting white contour frames around dark spots. Due to an inhomogeneous growth, no checker-board and consequently no clear in-plane easy axis can be identified. By applying a 0.2 T perpendicular external magnetic field, out-of-plane domains start to nucleate and the previous dark spots split into bubbles (see the circle of figure 6(b)). This is an indication that in LCMO/STO at low temperatures, it takes more energy to move the walls enlarging domains than to nucleate. The domain marked with a circle clearly splits into more. Saturation is reached at $H = 2$ T in agreement with the *ex situ* VSM measured out-of-plane hysteresis figure 6(d).

3. Artificial ferromagnetic/superconducting heterostructures

The interest in realization of the magnetic devices has driven physicists to fabrication of heterostructures constituted by a manganite and a material with similar structural parameters. This research has increased understanding of manganites and high-T_c superconducting cuprates, in particular $YBa_2Cu_3O_7$ (YBCO), heterostructures. These systems are interesting for their possible applications and for studying the interaction between magnetism and superconductivity.

3.1. YBCO/LCMO bilayers

The LCMO/YBCO and YBCO/LCMO have been deposited by a dc sputtering technique under high pressure of pure oxygen from stoichiometric targets. The oxygen pressure was 3.0 mbar and the temperature of the substrate was kept at 900 °C for

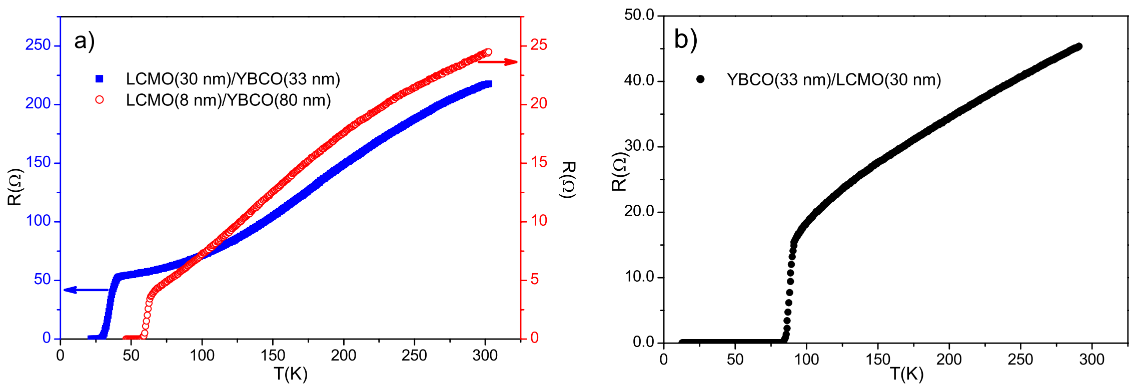

Figure 9. R versus T for LCMO/YBCO bilayer (a) with different thicknesses (b) R versus T for YBCO/LCMO bilayer.

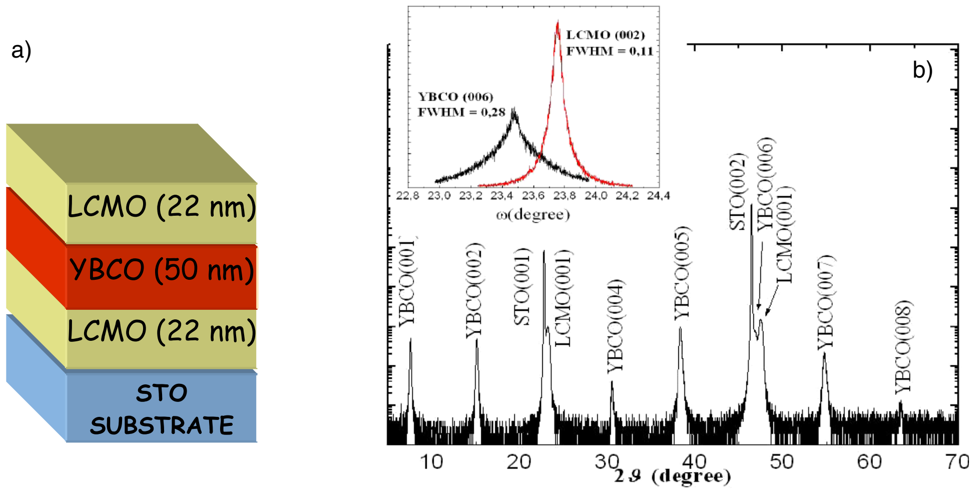

Figure 10. (a) Scheme of the trilayer. (b) The $\theta/2\theta$ XRD of a LCMO/YBCO/LCMO trilayer grown on $SrTiO_3$, in the inset: corresponding rocking curve.

both the LCMO and YBCO layers. After deposition, the thin films were treated by *in situ* annealing in a pure oxygen atmosphere at 560 °C for a minimum time of 10 min. The growth rate for YBCO was about 16.7 Å min^{-1} and our single layers of YBCO present a critical temperature $T_{CS}(\rho = 0) = 91$ K. The LCMO/YBCO and YBCO/LCMO bilayers have been characterized by x-ray measurements [11]. As we show in figure 7, in the patterns we observe only YBCO, LCMO and STO (00l) reflections, indicating that each layer has the *c*-axis perpendicular to the substrate surface. Moreover, we underline that the fact that reflections in LCMO/YBCO are not well defined in comparison with those of YBCO/LCMO. So we can affirm that the LCMO grows on YBCO less epitaxial than on a STO substrate. TEM analysis, in agreement with the x-ray measurements, confirms that both interfaces are very sharp, as we show in the high resolution electron microscopy image of the YBCO(55 nm)/LCMO(30 nm)/STO bilayer in figure 8.

In figures 9(a) and (b) we show the resistance versus temperature behavior for LCMO/YBCO and YBCO/LMCO heterostructures. We notice that, for the same thicknesses of the YBCO and the LCMO layers, we have different superconducting critical temperatures depending on the position of the two layers. In particular, if the YBCO is the top layer we notice that $T_{CS} \simeq 73$ K is lower than for the configuration with the LCMO as the top layer, in this case $T_{CS} \simeq 30$ K. Moreover, in both cases, we see a T_{CS} lower than the critical temperature of the YBCO layer of 91 K. The reduction of the superconducting critical temperature can be explained in terms of the injection of spin-polarized electrons from LCMO to YBCO. In fact if we reduce the thickness of the LCMO and increase the YBCO layer thickness, we notice, in the LCMO/YBCO bilayer, an increase in T_{CS} (figure 9(a) red dots).

3.2. LCMO/YBCO/LCMO trilayers

To continue our study of the coexistence between ferromagnetism and superconductivity, we have fabricated and characterized LCMO(23 nm)/YBCO (50 nm)/LCMO (23 nm) trilayers [12].

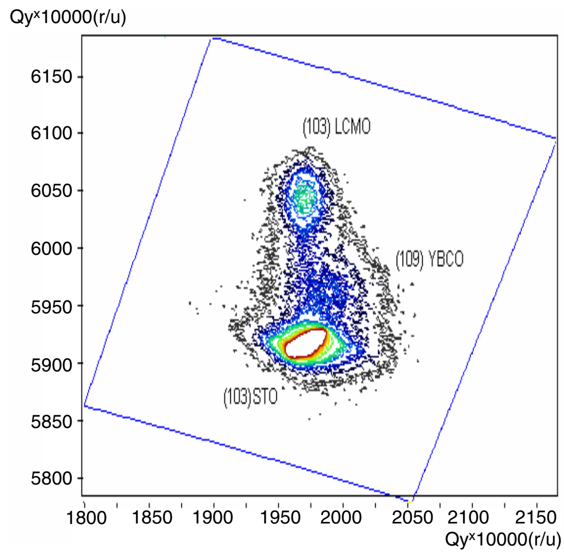

Figure 11. The asymmetric reciprocal space map of a LCMO(22 nm)/YBCO(50 nm)/LCMO(22 nm) trilayer illustrates the epitaxial growth of our heterostructures, showing that the in-plane axes of the substrate and of the LCMO and YBCO layers are all in the same direction.

In order to study the crystal structure of the different layers and the epitaxial relationship between them and the substrate, in-plane and out-of-plane x-ray diffraction measurements have been performed. In figure 10 the $\theta/2\theta$ spectrum is reported, showing that the substrate and the layers are all (00l) oriented. The epitaxial growth is confirmed by the in-plane *h*–*l* reciprocal map, as reported in figure 11, which shows that the in-plane axes of the substrate and the LCMO and YBCO layers are in the same direction. As shown in the inset of figure 10 we found that FWHM is 0.28° for YBCO and 0.11° for LCMO, indicating the epitaxiality of both layers. The resistivity versus temperature dependence of the trilayer [13], illustrated in figure 12(a), shows the onset of the superconducting transition at $T_C^S \simeq 35$ K, while in the normal state a nonlinear behavior is observed that, in

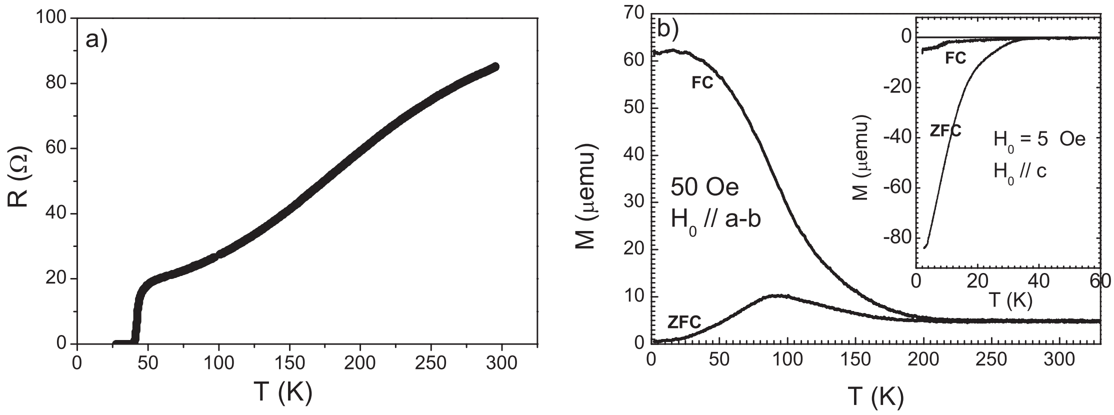

Figure 12. (a) R versus T measurement on LCMO(23 nm)/YBCO(50 nm)/LCMO(23 nm) trilayer. (b) M versus T behavior in zero field cooling (ZFC) and in field cooling (FC), applying a magnetic field of 50 Oe parallel to the *a*–*b* plane. In the inset we show M versus T measurements in ZFC and in FC, applying a magnetic field of 5 Oe parallel to the *c*-axis.

comparison with the single YBCO film, reflects the influence of the LCMO layers. On the same sample we have performed $M(T)$ measurements, both in zero field cooling mode (ZFC) and in field cooling (FC). An external magnetic field (H_0) of 50 Oe was applied parallel to the *a*–*b* plane of the STO substrate. From the $M(T)$ behavior (figure 12(b)) we infer a Curie temperature $T_C > 200$ K, higher than the T_C of a single LCMO film. In order to test the bulk features of the superconductivity in the YBCO layer we performed a new set of ZFC and FC measurements applying a magnetic field of 5 Oe, parallel to the substrate *c*-axis. As shown in the inset of figure 12(b), the experimental data indicate a T_C^S onset at around 35 K in agreement with the value reported by transport measurements.

4. Conclusions

We reported the structural, electrical and magnetic characterization of the LCMO thin films and of the LCMO/YBCO heterostructures. Major attention has been dedicated to the study of the dynamics of the magnetic domains in LCMO thin films by means of low temperature MFM. Using a Co/Cr coated cantilever, we probed the magnetic stray field above the sample surface. We analyzed the effects of different substrate induced strains considering the cases of NGO, ALO and STO single crystal substrates, respectively.

References

[1] Meissner W and Ochesenfeld R 1933 *Naturwissenschaften* **21** 787
[2] Prinz G A 1995 *Phys. Today* **48** 58
[3] Tokura Y (ed) 2000 *Colossal Magneto-Resistive Oxides* (The Netherlands: Gordon and Breach)
[4] De Santis A, Bobba F, Boffa M A, Caciuffo R, Mengucci P, Salvato M, Vecchione A and Cucolo A M 2004 *Physica* C **408** 48
[5] De Santis A 2003 *PhD Thesis* University of Salerno
[6] Salvato M, Vecchione A, Santis A D, Bobba F and Cucolo A M 2005 *J. Appl. Phys.* **97** 103712
[7] Ziese M, Semmelhackand H and Han K H 2003 *Phys. Rev.* B **68** 13444
[8] Rao R A, Lavric D, Nath T K, Eom C B, Wu L and Tsui F 1998 *Appl. Phys. Lett.* **74** 3636
[9] Bibes M, Valencia S, Balcells L I, Martnez B, Fontcuberta J, Wojcik M, Nadolski S and Jedryka E 2002 *Phys. Rev.* B **66** 134416
[10] De Santis A, Bobba F, Cristiani G, Cucolo A M, Frohlich K, Habermeierb H U, Salvato M and Vecchione A 2003 *J. Magn. Magn. Mater.* **262** 150
[11] Santis A D, Bobba F, Boffa M A, Caciuffo R, Mengucci P, Salvato M, Vecchione A and Cucolo A M 2004 *Physica* C **408–410** 48
[12] Salvato M, Bobba F, Calabrese G, Cirillo C, Cucolo A M, Santis A D, Vecchione A and Attanasio C 2006 *Eur. Phys. J.* B **51** 79
[13] Santis A D, Zola D, Piano S, Bobba F, Giubileo F, Longobardi M, Polichetti M, Pace S and Cucolo A M 2008 at press